Atf4 Regulates Obesity, Glucose Homeostasis, and Energy Expenditure

Jin Seo,[1] Edgardo S. Fortuno III,[1] Jae Myoung Suh,[1] Drew Stenesen,[1] Wei Tang,[1] Elizabeth J. Parks,[2] Christopher M. Adams,[3] Tim Townes,[4] and Jonathan M. Graff[1,2,5]

OBJECTIVE—We evaluate a potential role of activating transcription factor 4 (Atf4) in invertebrate and mammalian metabolism.

RESEARCH DESIGN AND METHODS—With two parallel approaches—a fat body–specific green fluorescent protein enhancer trap screen in *D. melanogaster* and expression profiling of developing murine fat tissues—we identified Atf4 as expressed in invertebrate and vertebrate metabolic tissues. We assessed the functional relevance of the evolutionarily conserved expression by analyzing *Atf4* mutant flies and *Atf4* mutant mice for possible metabolic phenotypes.

RESULTS—Flies with insertions at the *Atf4* locus have reduced fat content, increased starvation sensitivity, and lower levels of circulating carbohydrate. *Atf4* null mice are also lean, and they resist age-related and diet-induced obesity. *Atf4* null mice have increased energy expenditure potentially accounting for the lean phenotype. *Atf4* null mice are hypoglycemic, even before substantial changes in fat content, indicating that Atf4 regulates mammalian carbohydrate metabolism. In addition, the Atf4 mutation blunts diet-induced diabetes as well as hyperlipidemia and hepatosteatosis. Several aspects of the Atf4 mutant phenotype resemble mice with mutations in components of the target of rapamycin (TOR) pathway. Consistent with the phenotypic similarities, *Atf4* null mice have reduced expression of genes that regulate intracellular amino acid concentrations and lower intracellular concentration of amino acids, a key TOR input. Further, *Atf4* mutants have reduced S6K activity in liver and adipose tissues.

CONCLUSIONS—Atf4 regulates age-related and diet-induced obesity as well as glucose homeostasis in mammals and has conserved metabolic functions in flies. ***Diabetes*** **58:2565–2573, 2009**

The ability to sense nutrient availability and regulate energy homeostasis is an ancient and fundamental process that, when disturbed, leads to significant metabolic derangements (1). Modern life has provided unparalleled access to food, contributing to unprecedented proportions of obesity, insulin resistance, and diabetes (1). Epidemiological evidence implicates not only increased fat consumption but also excess protein intake as causative in the intertwined epidemics of obesity and diabetes (2). Further, human trials show that amino acid infusions induce insulin resistance (3). Two evolutionarily conserved pathways, target of rapamycin (TOR) and the integrated stress response (ISR), play central roles in responding to amino acid availability (4,5).

The mechanisms whereby surplus food consumption engenders insulin resistance are an area of intense scrutiny, and several lines of evidence implicate TOR signaling as an important contributor (6). TOR signals, which couple amino acid supplies to translational efficiency, are in part conveyed through ribosomal S6 protein kinase (S6K) and eukaryotic initiation factor 4E (eIF4E) binding protein 1 (4E-BP1) (4). Recent data indicate that this evolutionarily conserved cascade links nutrient excess to insulin resistance in flies and mammals (7–10). For example, flies with mutations in *4E-BP* or *TOR* control fat metabolism, and the *TOR* mutants have reduced lipid and glucose levels (7,8). Similarly, strains of *4E-BP1* mutant mice and *S6K* mutant mice are lean and have increased energy expenditure (9,10).

ISR is another highly conserved pathway that is important in translational control, nutrient sensing, and glucose homeostasis (11–13). The ISR is one branch of a signaling system termed the unfolded protein response (UPR) (12). Described for its role in handling stress induced by high demand of protein translation, for example during anabolic states, recent studies illuminate the notion that UPR has additional roles in metabolic physiology (11–13). For example, excessive UPR signaling leads to obesity, metabolic dysfunction, and fatty liver (14). Atf4, a bZip transcription factor, is an important component of the ISR (5). In the liver other bZip factors, C/EBPs, connect the ISR to several important metabolic functions, such as lipid, glucose, and glycogen biosynthesis, by increasing the expression of genes such as peroxisome proliferator–activated receptor γ (PPARγ) (14). The stress pathway is thought to have adaptive responses but if prolonged or excess can lead to maladaptive metabolic changes. For instance, a variety of animal studies indicate that excess stress, for example induced by knockouts of components of the UPR that rectify stress, can lead to obesity and fatty liver (15). Although the role of Atf4 in metabolic control is yet to be defined, it is known that Atf4 plays a central function in handling stress induced by amino acid imbalances (5). In addition, Atf4 regulates memory formation and is required for the appropriate development of cell lineages including blood and bone (16–18). The bone defects can be corrected by feeding the mutant animals a high protein diet, indicating that the roles of Atf4 in bone formation are nutritionally linked (19).

From the [1]Department of Developmental Biology, University of Texas Southwestern Medical Center, Dallas, Texas; the [2]Department of Internal Medicine, University of Texas Southwestern Medical Center, Dallas, Texas; the [3]Department of Internal Medicine, Roy J. and Lucille A. Carver College of Medicine, The University of Iowa, Iowa City, Iowa; the [4]Department of Biochemistry and Molecular Genetics, University of Alabama at Birmingham, Birmingham, Alabama; and the [5]Department of Molecular Biology, University of Texas Southwestern Medical Center, Dallas, Texas.

Corresponding author: Jonathan M. Graff, jon.graff@utsouthwestern.edu.

Received 9 March 2009 and accepted 28 July 2009. Published ahead of print at http://diabetes.diabetesjournals.org on 18 August 2009. DOI: 10.2337/db09-0335.

A variety of recent data indicate that the regulatory cascades controlling metabolism are conserved among evolutionarily diverse organisms such as worms, flies, and mammals (20). To attempt to isolate genes involved in metabolism, we characterized and compared the molecular signature of fly and murine developing metabolic tissues with the premise that conserved genes expressed in both organisms were plausible candidates. In *D. melanogaster*, we undertook an enhancer trap screen to isolate genes expressed in the larval fat body, a central fly metabolic organ (21), and identified *Atf4*. We also found that Atf4 was expressed in the embryonic day 14.5 (E14.5) mammalian fat anlagen using a combinatorial transgenic-transcriptional profiling approach. The evolutionarily conserved expression may have functional relevance because both *Atf4* mutant flies and *Atf4* null mice are lean and have reduced levels of circulating carbohydrate. The *Atf4* mutant mice resist diet-induced and age-dependent obesity and diabetes. Further, the *Atf4* mutant mice have increased energy expenditure. Liver and adipose tissues, key metabolic organs, removed from the *Atf4* mutant mice have reduced expression of genes controlling intracellular amino acid concentrations. Further, tissues of *Atf4* mutants contained lower amino acid levels, thereby supporting the idea that changes in amino acid metabolism are present in vivo. These tissues also have decreased activity of the TOR signaling pathway, which responds to amino acid inputs. These data support the notion that Atf4 is a conserved regulator of metabolism and carbohydrate homeostasis, thus providing a mechanistic link between nutrients, insulin resistance, and diabetes.

RESEARCH DESIGN AND METHODS

Fly studies. The X-linked enhancer trap P-element, PGawB, was mobilized to generate new insertions as described previously (22). Individual F1 larvae were screened for fat body green fluorescent protein (GFP) expression under a fluorescence-dissecting microscope, and fat body enhancer trap lines were established by crossing to balancer stocks. Adult fat body tissues were explanted under dissected microscopy, placed in PBS, and photographed with differential interference contrast or fluorescence microscopy as described (20). Insertion sites were identified by inverse PCR and/or plasmid rescue. Starvation and triglyceride assays were performed as described (20). For trehalose quantification, 2 μl of pooled hemolymph from L3 larvae was collected, diluted, heat inactivated, and treated with porcine kidney trehalase (Sigma). Glucose concentration was measured using Infinity Glucose Reagent (ThermoElectron). For Nile Red staining, whole flies or dissected fat bodies were fixed in formalin, permeabilized in 0.2% Triton X-100 solution, stained with Nile Red, and documented under a fluorescence-dissecting scope as described (20).

Mouse studies. The aP2-GFP mice were generated by placing GFP into the 5.4-kb aP2 enhancer/promoter (23). Multiple transgenic lines were generated and screened for GFP expression in embryonic and adult fat depots with fluorescent microscopy. For this study, we selected the transgenic strain with the highest, most specific, and most consistent expression of GFP in embryonic and adult fat tissues. RNA was extracted from GFP-negative and -positive cells either after careful dissection or after dissociation and fluorescence-activated cell sorter (FACS). The Affymetrix microarrays were done by the University of Texas Southwestern Microarray Core Facility (http://microarray.swmed.edu). *Atf4* heterozygous mice were backcrossed with pure inbred C57BL/6 mice, housed, and analyzed as described (18,20). Mice were fed either normal (4% fat, Teklad) or high-fat chow (60% fat, Research Diets). Fat content was measured using a minispec mq10 NMR Analyzer (Bruker). For glucose tolerance tests and insulin tolerance tests, 1.25 mg glucose or 0.9 mU Humulin R (Lilly)/1g body wt was injected intraperitoneally, and blood glucose levels were measured at the indicated intervals as described (20). Veterinary care was provided by the Division of Comparative Medicine. All animals were maintained under the guidelines of the University of Texas Southwestern Medical Center Animal Care and Use Committee according to current National Institutes of Health guidelines.

Histological studies. Tissues from *Atf4* null and control mice were fixed with formalin solution, dehydrated with tissue processor (Microm), and embedded in paraffin. Hematoxylin-eosin was used to cut and stain 5- to 8-micron sections. For in situ hybridizations, embryos were collected from C57BL/6 female mice at E14.5, fixed in formalin, dehydrated, embedded in paraffin, and 5-micron sections hybridized with α-^{32}P-[UTP]–labeled antisense aP2 or *Atf4* probe.

RNA extractions and real-time PCR. Total RNA was extracted using TRIzol (Invitrogen), DNaseI treated, and reverse transcribed with random hexamers. Gene expression was analyzed using 7500 Real-Time PCR System (Applied Biosystems) using SYBR Green Master Mix reagent (Applied Biosystems). The values for gene expression were normalized by β-actin expression. Primer sequences are available upon request.

Western blotting and antibodies. Immunoblotting was performed according to standard procedures. Protein samples were extracted using phosphoSafe Extraction Reagent (Calbiochem), boiled, and separated on denaturing polyacrylamide gels (percentage varied from 8–15%) prior to transfer onto nitrocellulose. The membrane was blocked and incubated with primary antibodies. Primary antibodies were purchased from the following: β-actin (Sigma), SLC1A4 (Millipore), uncoupling protein (UCP)-1 and AARS (Abcam), and all other antibodies (Cell Signaling Technology). Subsequently, the nitrocellulose membranes were washed and incubated with secondary antibodies conjugated with horseradish peroxidase (Jackson Immunoresearch). Signals are detected with chemiluminescent kits (NEN).

Lipid extraction, gas chromatography, and fatty acid composition. Floating adipocytes were isolated from control and *Atf4* mutants as described (24). Total lipids were extracted for lipid analysis. Trinonadecanoin and pentadecanoic acid were used as internal standards for analysis by gas chromatography. Palmitoleate composition of the triglyceride fraction was determined by gas chromatography with flame-ionization detection, and the identity was determined by retention time and compared with the internal standard for quantification.

Measurement of intracellular free amino acid concentration. Protein concentrations of plasma mixed with 5% trichloroacetic acid and homogenized high-fat diet–fed mouse tissues were determined, and then the samples were centrifuged. The supernatant was filtered through 0.2 μm polytetrafluoroethylene centrifuge filter to remove precipitated proteins and tissue debris. Free amino acid concentrations of the samples were analyzed using a Hitachi L-8800 amino acid analyzer (25).

Measurement of intracellular cAMP. cAMP concentration was measured using Cyclic AMP Assay Kit (R&D) according to the manufacturer's protocol. Brown adipose tissue (BAT) was homogenized using phosphoSafe Extraction Reagent (Calbiochem). cAMP concentration of each BAT sample was determined by comparing with the cAMP standard curve with duplicates of each protein sample (50 μg).

RESULTS

dAtf4 is expressed in the developing and adult *D. melanogaster* fat body. To identify genes that might regulate metabolism, we characterized the molecular signature of the *D. melanogaster* larval fat body, a central fly metabolic organ. We performed a two-component (minimal promoter Gal4; upstream activating sequence–GFP) enhancer trap insertional screen (22) and isolated ~600 lines with fat body GFP expression. This produced a set of 587 genes including many previously reported to be fat body specific (e.g., *Adh*, *arg*, and *vkg*). Remarkably, although redundant insertions were quite uncommon, two of the fat body enhancer trap lines, E8 and G74, had insertions at the CG8669 locus, encoding the fly homolog of *Atf4* (Fig. 1*A*) (26). In larvae, E8 expression appeared relatively specific to the fat body, whereas G74 also had ectoskeletal coexpression; both lines also displayed strong expression in adult metabolic tissues (Fig. 1*B*).

mAtf4 is expressed in embryonic and adult murine fat tissues. We also found that Atf4 was expressed in E14.5 murine metabolic tissues in a screen combining fluorescent cell–marking techniques, FACS, and microarray technology. This was based upon the observations that aP2, a known marker of adult fat depots, had restricted expression in the E14.5 fat pad (Fig. 1*C*) (23) and that aP2-GFP transgenic mice had strong GFP expression in embryonic fat tissues (Fig. 1*D*). The latter facilitated isolation of pure

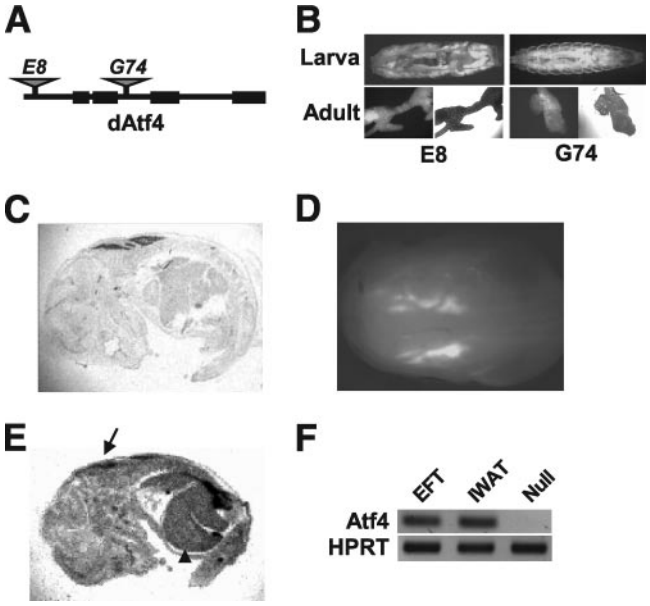

FIG. 1. Atf4 is expressed in fly and mammalian metabolic tissues. *A*: Schematic diagram of E8 and G74 insertions at the CG8669 locus encoding the fly Atf4 homolog (dAtf4). *B*: The E8 and G74 enhancer trap lines express upstream activating sequence–GFP in the larval (*top*) and adult (*bottom*) fat body. *Lower right* panels show differential interference contrast image of the adult fat body explants. *C*: aP2 in situ hybridization on a parasagittal section of an E14.5 mouse embryo. *D*: Dorsal view of an E14.5 aP2-GFP transgenic embryo viewed with fluorescence microscopy. *E*: Atf4 in situ hybridization on E14.5 mouse embryo. The arrow highlights Atf4 expression in the E14.5 fat pad, and the arrowhead identifies liver expression. *F*: RT-PCR of cDNA derived from the embryonic fat tissue (EFT) of wild-type (*left lane*) and *Atf4* null (*right lane*) mice and adult inguinal wild-type WAT (IWAT, *middle lane*) mice. HPRT (hypoxanthine phosphoribosyl transferase) serves as a loading control.

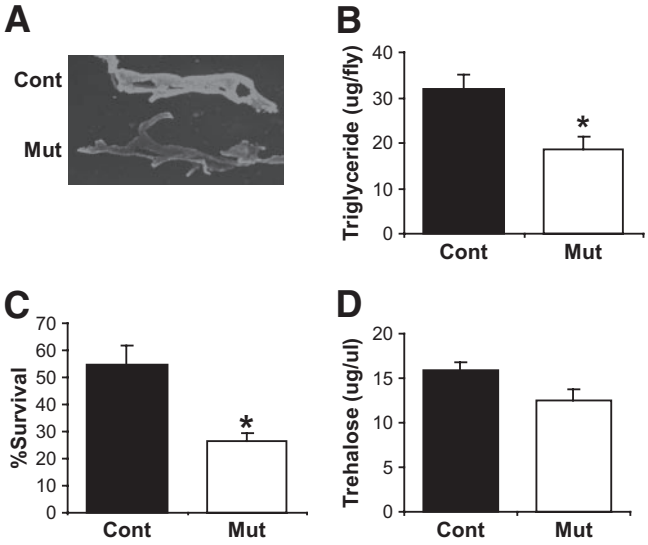

FIG. 2. Atf4 regulates fly metabolism. *A*: Photo of Nile Red–stained (fat stains red) E8 *dAtf4* insertional mutant (Mut) and control (Cont) larval fat body. *B*: Triglyceride levels of G74 *dAtf4* insertional mutants and controls ($n \geq 40$). *C*: Day 5 starvation survival of G74 *dAtf4* insertional mutants and controls ($n \geq 40$). *D*: Trehalose levels of E8 larvae of *dAtf4* insertional mutants and controls ($n \geq 40$). Error bars indicate SEM. Statistical significance was assessed by two-tailed Student *t* test. $^*P < 0.05$.

populations of E14.5 GFP^+ and GFP^- cells using dissections and FACS. We performed a series of Affymetrix microarray experiments to identify genes upregulated in GFP^+ cells compared with GFP^- cells. We then compared those genes expressed in the E14.5 fat anlagen with those identified in the fly enhancer trap screen; *Atf4* was on both lists. In situ hybridizations and RT-PCR analyses showed that Atf4 was expressed in embryonic fat depots in the developing liver, a key metabolic tissue, and also in adult fat depots (Fig. 1*E* and *F*).

***Atf4* mutant flies are lean and have reduced circulating carbohydrate levels.** To determine whether the expression of Atf4 in fly metabolic tissues might have functional relevance, we examined the phenotype of the flies with P-element insertions at the *Atf4* locus and found that they had altered metabolism. For example, E8 and G74 insertion mutant flies had reduced fat content based upon Nile Red staining of fat body explants, lower triglyceride levels, and increased starvation sensitivity (Fig. 2*A–C*). These flies also had a trend of reduced circulating levels of trehalose, the fly glucose equivalent (Fig. 2*D*).

***Atf4* mutant mice are lean and protected from age-related obesity.** The number of *Atf4* mutant offspring in the C57BL/6 (B6) background is reduced (8.9%; 15/168) compared with the expected Mendelian ratio, but mice surviving >3 months are healthy and 14% have smaller body length (control 9.4 ± 0.15 cm, $n = 8$; mutant 8.1 ± 0.22 cm, $n = 6$) (27). To evaluate a potential role of Atf4 in mammalian metabolism, we analyzed young adult cohorts (aged 3 months) of *Atf4* null and control siblings fed normal chow diet. Because aging is associated with increased insulin resistance and obesity (28,29), we also studied older mice (aged 12 months). Based upon appearance, nuclear magnetic resonance fat content analyses, and examination of adipose depots, the young adult *Atf4* mutants had modestly reduced fat mass compared with controls, and this effect substantially increased with age (Fig. 3*A–E*), indicating that the *Atf4* mutants resist age-associated obesity. However, kidney and heart weights, normalized to lean body mass, approximated those of controls (Fig. 3*F*, supplemental Table S1 in the online appendix, available at http://diabetes.diabetesjournals.org/content/early/2009/08/13/db09-0335/suppl/DC1). At young ages, *Atf4*-deficient adipocytes were of similar size to or in some cases even larger than control adipocytes. However, they had a blunted hypertrophic response to age-associated obesity (Fig. 3*G*).

***Atf4* mutant mice resist diet-induced obesity.** To examine the potential role that Atf4 may play in diet-induced obesity, we provided a high-fat diet to control and *Atf4* mutant littermates. During the 16 weeks of high-fat diet, we followed the mice with weekly weights, normalizing them to starting weight, and found that *Atf4* mutants had a significantly blunted response to high-fat diet (Fig. 4*A*). This resistance to diet-induced weight gain was accompanied by a marked decrease in fat accumulation as determined by nuclear magnetic resonance analyses as well as by gross observation and weights of fat depot explants (Fig. 4*B–E*). However, the weights of other organs were not affected (data not shown). The differences in fat content are apparent in histological sections, which show that although control mice have significant fat, *Atf4* null mice have a paucity of such deposition (Fig. 4*F*). In addition, the adipocytes are substantially smaller than those observed in controls (Fig. 4*F*). Fatty liver, a leading cause of liver disease, is a manifestation of metabolic dysfunction that can be elicited by high-fat diet (30). Consistent with that, we found that high-fat diet led to

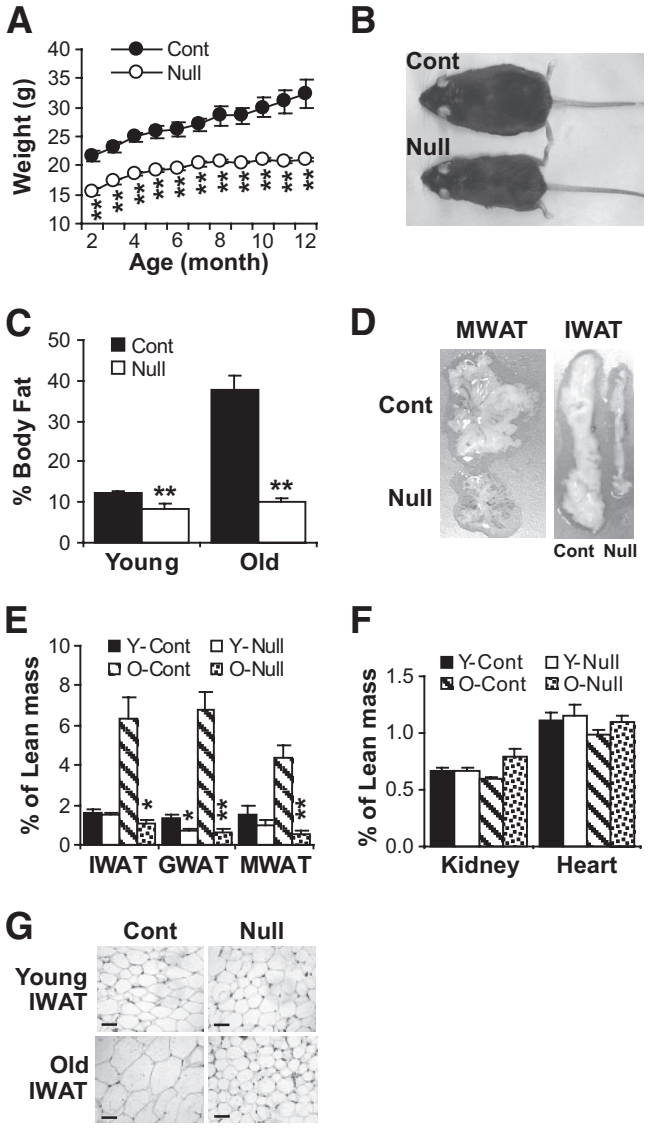

FIG. 3. ***Atf4*** **mutant mice are lean and resist age-associated obesity.** ***A*****: Serial weights of control (Cont) and** ***Atf4*** **null mice on normal chow diet.** ***B*****: Photograph of 1-year-old normal chow–fed control and** ***Atf4*** **null siblings.** ***C*****: Nuclear magnetic resonance body fat analyses of 3-month-old normal chow diet (young) and 12-month-old normal chow diet (old) control and** ***Atf4*** **null mice (**$n \geq 6$**).** ***D*****: Photograph of representative mesenteric WAT (MWAT) and inguinal WAT (IWAT) depots from 12-month-old normal chow–fed control and** ***Atf4*** **null littermates.** ***E*****: Average weight expressed as percentage of lean body mass of IWAT, perigonadal WAT (GWAT), and MWAT depots of 3-month-old (Y) and 12-month-old (O)** ***Atf4*** **null siblings (**$n \geq 6$**).** ***F*****: Average weight normalized to lean body mass of kidney and heart of 3-month-old (young) and 1-year-old (old) control and** ***Atf4*** **null mice (**$n \geq 6$**).** ***G*****: Histology of IWAT of 3-month-old and 1-year-old normal chow–fed control and** ***Atf4*** **mutant siblings (bar = 50 μm). Error bars indicate SEM. Statistical significance was assessed by two-tailed Student** ***t*** **test or repeated-measures ANOVA followed by Bonferroni post tests (***A***).** $^{*}P < 0.05$**;** $^{**}P < 0.01$**.**

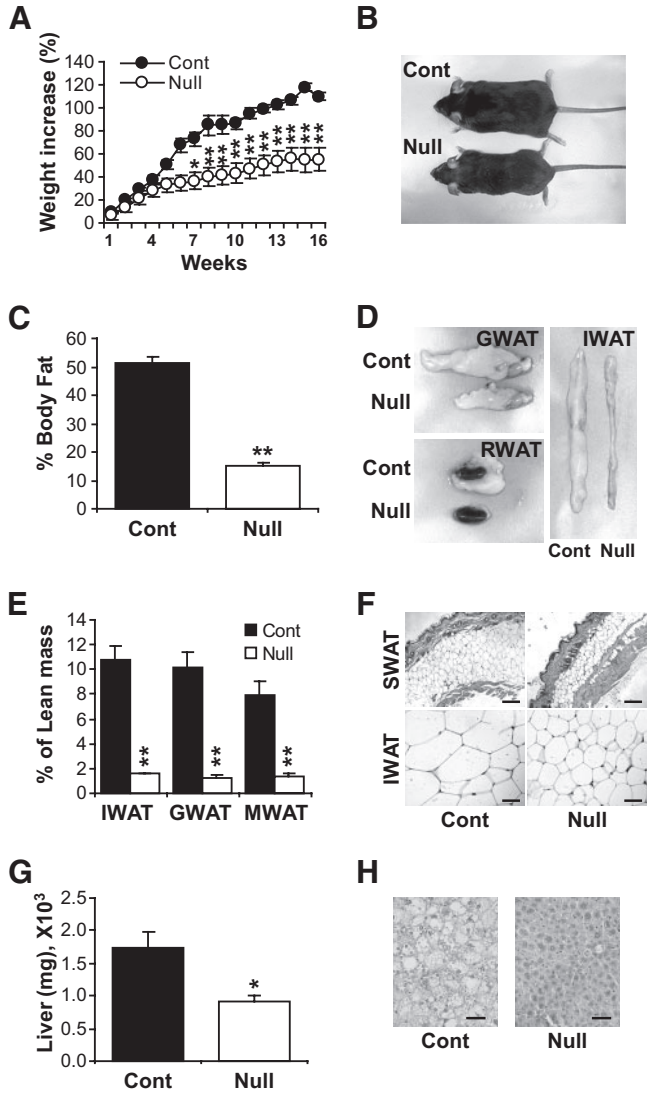

FIG. 4. ***Atf4*** **mutant mice are lean and resist age-associated and diet-induced obesity.** ***A*****: Serial weights of control (Cont) and** ***Atf4*** **null siblings on high-fat diet.** ***B*****: Photograph of representative control and** ***Atf4*** **mutant littermates after 16 weeks of high-fat diet.** ***C*****: Nuclear magnetic resonance body fat analyses of 6-month-old high-fat diet–fed control and** ***Atf4*** **null mice (**$n \geq 6$**).** ***D*****: Photograph of representative perigonadal WAT (GWAT), perirenal (RWAT), and inguinal WAT (IWAT) depots from high-fat diet–fed control and** ***Atf4*** **null littermates.** ***E*****: Average weights of IWAT, GWAT, and MWAT depots of 6-month-old high-fat diet control and** ***Atf4*** **null siblings (**$n \geq 6$**).** ***F*****: Histology of skin WAT (SWAT) and IWAT of high-fat diet control and** ***Atf4*** **mutant siblings (bar = 50 μm).** ***G*****: Liver weights of high-fat diet control and** ***Atf4*** **null siblings (**$n = 8$**).** ***H*****: Representative liver histology of high-fat diet control and** ***Atf4*** **nulls (bar = 50 μm). Error bars indicate SEM. Statistical significance was assessed by two-tailed Student** ***t*** **test or repeated-measures ANOVA followed by Bonferroni post tests (***A***).** $^{*}P < 0.05$**;** $^{**}P < 0.01$**.**

significant fat deposition in the livers of wild-type mice (Fig. 4*G*, H). In contrast, *Atf4* mutants were resistant to this pathology (Fig. 4*G* and *H*).

Atf4 **mutant mice are hypoglycemic.** Next we examined control and *Atf4* mutant siblings for aspects of glucose homeostasis and found that Atf4 regulated murine carbohydrate metabolism. For example, *Atf4* mutants had lower random and fasting glucose levels, and glucose tolerance tests showed that normal chow–fed *Atf4* null mice had improved glucose metabolism (Fig. 5*A*–*C*). Even at the young ages, the *Atf4* mutant cohorts displayed glucose levels and glucose tolerance test results that were reduced compared with controls (Fig. 5*B*) and seemingly out of proportion to the relatively modest changes in fat content observed at these ages (Fig. 3*C*). This may indicate that Atf4 has direct functions in glucose metabolism that are independent of the degree of fat reduction. In support of that notion, we found that insulin levels in normal chow–fed *Atf4* mutants approximated control levels (Fig. 5*D*). This normal insulin level, in the setting of lowered blood glucose, indicates relative insulin excess and may be

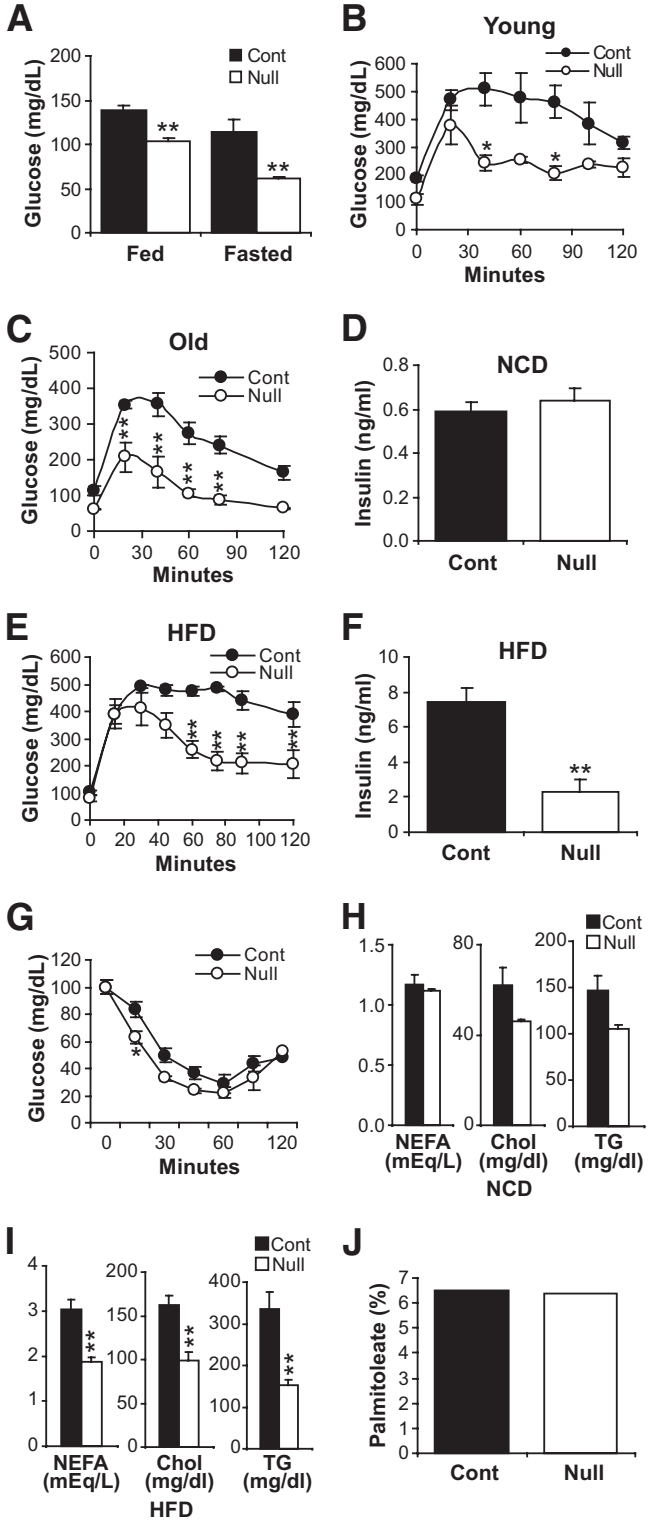

FIG. 5. *Atf4* deficiency alters glucose metabolism. *A*: Random and fasting glucose levels of normal chow–fed control (Cont) and *Atf4* null siblings ($n \geq 6$). *B* and *C*: Glucose tolerance tests of 3-month-old (young, *B*) and 1-year-old (old, *C*) normal chow–fed control and *Atf4* mutants ($n \geq 6$). *D*: Insulin levels of young control and *Atf4* null siblings on normal chow diet (NCD) ($n \geq 6$). *E*: Glucose tolerance tests of control and *Atf4* mutants on high-fat diet (HFD) ($n \geq 6$). *F*: Insulin levels of control and *Atf4* null siblings on high-fat diet ($n \geq 6$). *G*: Insulin tolerance tests of control and *Atf4* null siblings ($n = 8$). *H* and *I*: Average plasma levels of nonesterified fatty acid (NEFA), cholesterol (Chol), and triglyceride (TG) in normal chow diet (*H*) and high-fat diet (*I*) control and *Atf4* mutant littermates ($n \geq 6$). *J*: Palmitoleate ratio of adipocyte (isolated by floatation) triglycerides of control and *Atf4* nulls ($n = 3$). Error bars indicate SEM. Statistical significance was assessed by two-tailed Student *t* test or repeated-measures ANOVA followed by Bonferroni post tests (*B*,*C*, *E*, and *G*). *$P < 0.05$; **$P < 0.01$.

consistent with the previously identified role of the ISR in β-cell apoptosis, proliferation, and insulin secretion (31–33).

The *Atf4* mutation also ameliorated high-fat diet–induced hyperglycemia (Fig. 5*E*). However, in this setting insulin levels were significantly lower than those for controls (Fig. 5*F*), pointing to roles of Atf4 in metabolism that are independent of the pancreas and potentially related to the lean phenotype described above. An insulin tolerance test indicated that the *Atf4* mutant mice were insulin sensitive (Fig. 5*G*). Diet-induced and age-related obesity can provoke hyperlipidemia (1). The *Atf4* mutation appeared to ameliorate this adverse consequence as the high-fat diet *Atf4* null mice and the 12-month-old normal chow–fed mutants had improved lipid profiles compared with those for controls (Fig. 5*H* and *I*). Recent evidence indicates that the adipose-generated lipid palmitoleate is a lipokine that regulates glucose homeostasis (34). This does not appear to be the mechanism whereby Atf4 impacts metabolism because control and *Atf4* mutant fat depots had equivalent levels of this fatty acid (Fig. 5*J*).

***Atf4* mutant mice have increased energy expenditure.** To attempt to identify the basis of the lean phenotype, we examined eating behavior, activity, and metabolic rate comparing *Atf4* null and control siblings on either normal chow or high-fat diet. Food intake was equivalent in the *Atf4* mutants and controls (Fig. 6*A*). The leanness was not due to increased activity because X-Y movement (walking) was equivalent in the two groups and Z-axis (rearing) activity was reduced by *Atf4* deficiency (Fig. 6*B*). *Atf4* null mice did have increased energy expenditure, displaying a higher rate (~15% increase) of oxygen consumption (VO_2) in both light and dark phases that was accentuated by high-fat diet (~30% increase) (Fig. 6*C* and *D*). Because adipose tissue, reduced in *Atf4* mutants, and muscle have differential contributions to whole-body VO_2, we repeated the metabolic chamber analyses on additional cohorts of mice and in these cases with normalized energy expenditure using lean body mass. Again, *Atf4* mutant mice had elevated energy expenditure (Fig. 6*E* and *G*). We also plotted the absolute energy expenditure (a per mouse analysis, plotting lean mass vs. VO_2) of control and *Atf4* mutants, and the slopes are illustrated in supplemental Fig. S1 in the online appendix. Another indication of altered metabolism is the observation that *Atf4* mutants had a substantially lower respiratory quotient (RQ, VCO_2/VO_2), a measure of the proportionate rates of substrate utilization, indicating higher fat oxidation (Fig. 6*F*). Core body temperature is an additional measure of energy expenditure. Consistent with the other metabolic studies, we found that *Atf4* mutant mice had elevated core body temperature (Fig. 6*H*). Given the starvation sensitivity observed in the Atf4 mutant flies (Fig. 2*C*), we also measured respiratory quotient and VO_2 during the fed-to-fasted transition. Initially the respiratory quotients and VO_2s became similar, but with a sustained fast the mutant animal VO_2 dropped precipitously and the mutants become acutely ill. This indicates a potential defect in starvation resistance, reminiscent of fly starvation intolerance (Figs. 2*C*, 6*F*, and 6*G*). Next we investigated potential energy expenditure defects molecularly. Levels of per-

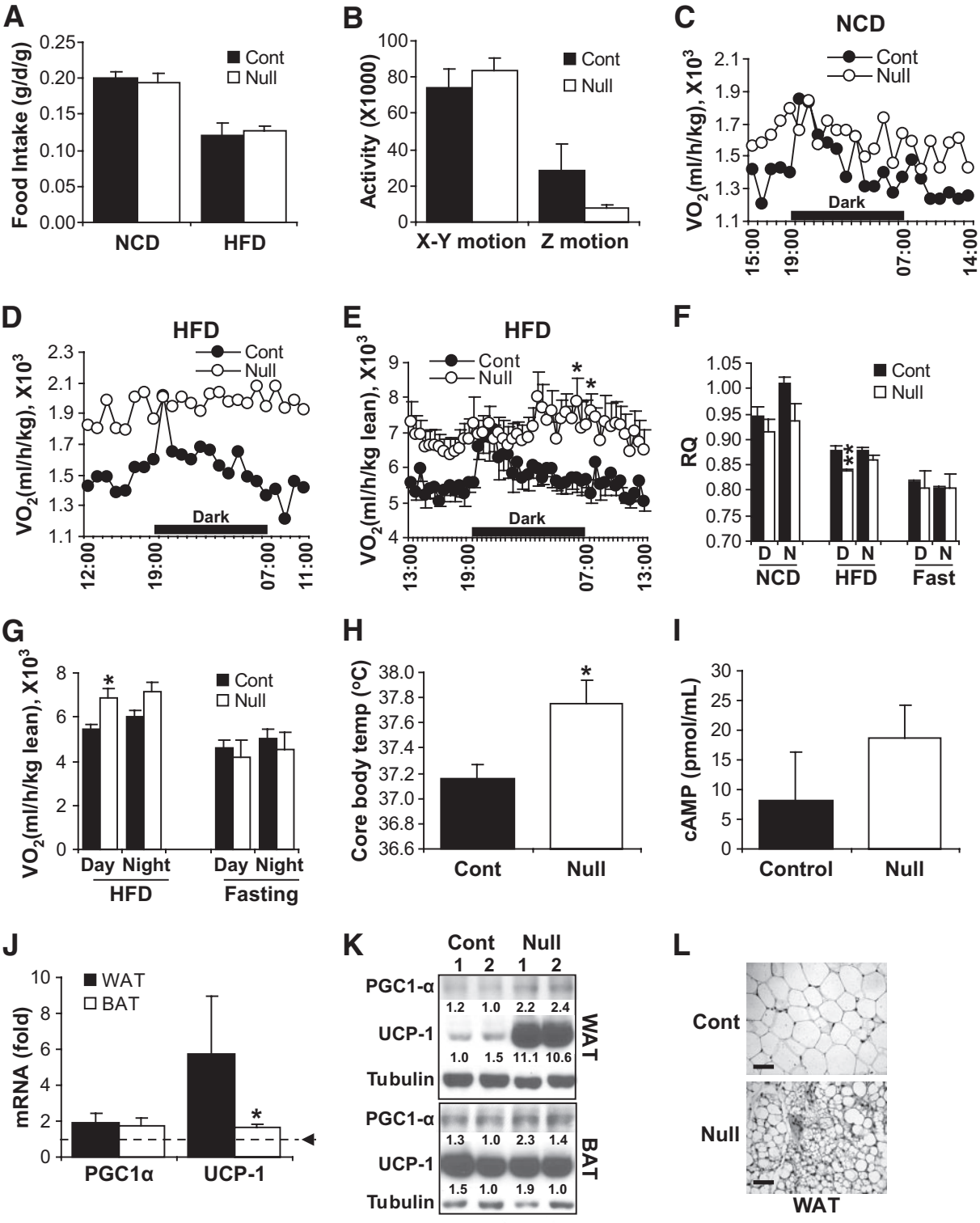

FIG. 6. ***Atf4*** **mutant mice have increased energy expenditure.** ***A*****: Food intake of control (Cont) and** ***Atf4*** **null siblings (*n* = 12). Food intake was normalized by mouse body weight.** ***B*****: Activity of control and** ***Atf4*** **null mice (*n* = 12).** ***C*****,** ***D*****, and** ***E*****: Oxygen consumption of control and** ***Atf4*** **null siblings provided a normal chow diet (NCD) (*C*) or high-fat diet (HFD) (*D* and *E*) (*n* = 2). Oxygen consumption was normalized by total body weight (*C* and *D*) or by lean body mass (*E*).** ***F*****: Average respiratory quotient (RQ) of control and** ***Atf4*** **null siblings fed a normal chow diet or a high-fat diet and fasting (*n* = 12) during the day (D) and the night (N).** ***G*****: Average oxygen consumption of control (wild type) and** ***Atf4*** **null siblings on a high-fat diet or upon fasting (*n* = 12).** ***H*****: Core body temperature of control and** ***Atf4*** **null siblings (*n* ≥ 6).** ***I*****: cAMP levels of control and** ***Atf4*** **null siblings in BAT extracts (*n* = 6).** ***J*****: Relative expression of energy expenditure genes in WAT and BAT of** ***Atf4*** **mutants compared with control siblings (*n* ≥ 6). Dotted line and arrowhead indicate wild-type control expression.** ***K*****: Western blots of metabolic proteins in WAT and BAT extracts. Quantification, number below the band, was determined using ImageJ software and normalized to tubulin, a loading control.** ***L*****: Histology of mesenteric WAT of 1-year-old normal chow diet–fed mice (bar = 50 μm). Error bars indicate SEM. Statistical significance was assessed by two-tailed Student *t* test or repeated-measures ANOVA (*C*, *D*, and *E*) followed by Bonferroni post tests. *$P < 0.05$.**

oxisome proliferator–activated γ coactivator (PGC)-1α, UCP-1, and/or cAMP often reflect metabolic rate. We determined their expression or concentration in adipose tissues. First, we examined cAMP levels in BAT, a major source of thermogenesis. We observed a trend toward increased cAMP concentrations in *Atf4* mutant mice (Fig. 6*I*), possibly reflecting increased metabolic activity. Next, we quantified mRNA levels in BAT and white adipose tissue (WAT) using qPCR. Expression of some genes involved in mitochondrial biogenesis and energy expenditure (e.g., PGC1-α and UCP-1) was slightly increased in *Atf4* mutant BAT and WAT (Fig. 6*J*). We then examined the levels of these two proteins using Western blots. We found that PGC1-α, a key transcriptional regulator of oxidative capacity, was modestly increased in both tissues with a greater increase in WAT. Notably, the Western blots revealed a marked increased (~10-fold) in UCP-1 protein levels (often thought of as a marker of BAT) in *Atf4* mutant WATs (Fig. 6*K*). Consistent with that observation, we found that *Atf4* mutant mice contained multilocular adipocytes, characteristics of BAT in WAT depots (Fig. 6*L*).

***Atf4* mutant mice have reduced TOR activity.** Several lines of evidence indicate that Atf4 regulates intracellular amino acid metabolism (5,25). Notably, high intake of amino acids leads to both adiposity and insulin resistance (2,3). In cellular assays, Atf4 siRNA reduces intracellular concentrations of amino acids (25). Because reduced amino acid availability could account for various aspects of the *Atf4* mutant phenotype (35), we assessed expression of genes important in intracellular amino acid concentrations in control and *Atf4* mutant mouse embryonic fibroblasts (MEFs) as well as adipose depots and livers because these two tissues are metabolically relevant and are affected by *Atf4* deficiency. Based upon qPCR, we detected significantly reduced levels of genes regulating amino acid metabolism, and transport was in *Atf4* mutant MEFs (Fig. 7*A* and *B*). We also measured protein levels of some of the salient genes. We found that alanyl-tRNA synthetase was significantly reduced, whereas solute carrier family 1 member 4 levels were equivalent. Both liver and adipose tissues from *Atf4* mutant mice also showed the same trends as those detected in the MEFs (Fig. 7*C* and *D*). We extended the data by directly quantifying amino acid concentrations in plasma, liver, and adipose depots of control and *Atf4* mutant siblings (Fig. 7*E* and supplemental Fig. S2 in the online appendix). Although plasma amino acid levels were comparable, the Atf4 mutant tissues displayed a trend toward reduced concentrations of amino acids. Several of the metabolic characteristics observed in the *Atf4*-deficient flies and mice mirror phenotypes observed when components of the TOR pathway are mutated in those organisms (7–10). These phenotypic similarities coupled with the Atf4-dependent regulation of amino acid availability, a key TOR input (5,36), prompted us to examine metabolic tissues of *Atf4* mutants and control siblings for TOR activity. Therefore, we assessed the phosphorylation of S6K, a key TOR target, in liver and adipose tissues removed from *Atf4* mutants and control siblings. We found that S6K phosphorylation was reduced in *Atf4* mutant liver and adipose tissues (Fig. 7*F*). We observed a similar reduction in the levels of phosphorylation of S6, an S6K target (Fig. 7*F*). To examine the possibility that the *Atf4* mutation might lead to a state of energy depletion and consequent altered TOR activity, we analyzed the activity of AMP-activated protein kinase, a central regulator and sensor of intracellular energy balance and changes in ATP levels (37). However, the levels of AMP-activated protein kinase phosphorylation in the activation loop were similar in control and *Atf4* mutant tissues (Supplemental Fig. S3 in the online appendix).

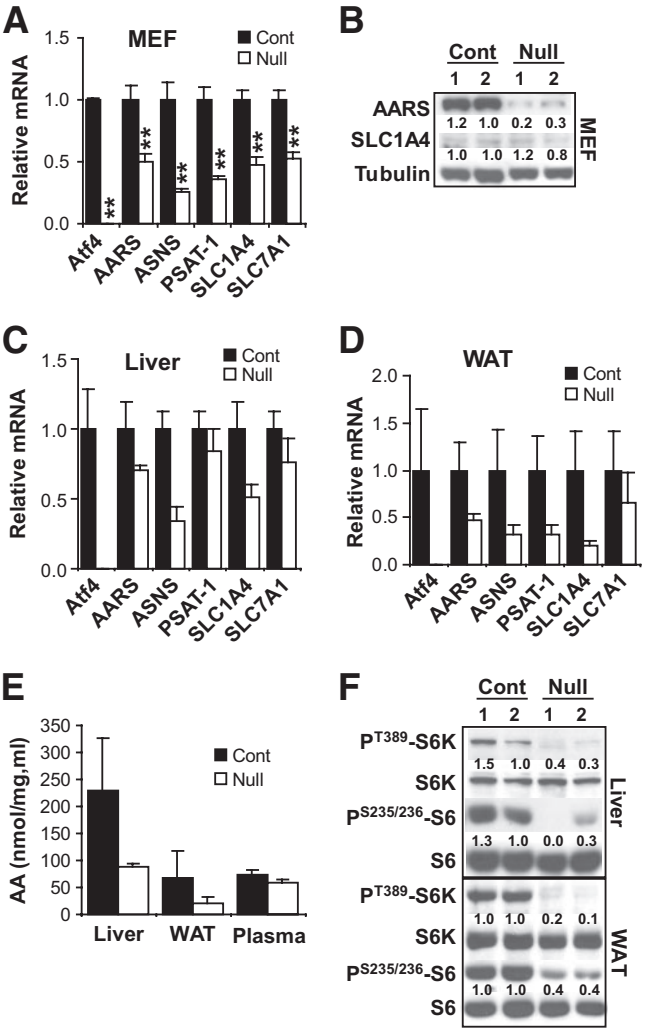

FIG. 7. *Atf4* mutant mice have reduced TOR activity. *A*, *C*, and *D*: qPCR analyses of genes that regulate intracellular amino acid levels in MEFs (*A*), liver (*C*), and adipose tissue (*D*) extracts of control and *Atf4* mutant siblings ($n \geq 6$). Asparagines synthetase (ASNS) and phosphoserine aminotransferase 1 (PSAT-1) are amino acid biosynthetic enzymes; alanyl-tRNA synthetase (AARS) is amino acid synthetase; solute carrier family 1 (glutamate/neutral amino acid transporter), member 4 (Slc1A4), solute carrier family 7 (cationic amino acid transporter, y+system), member 1 solute carrier family 7 (cationic amino transporter, y+system), and member 1 (Slc7A1) are amino acid transporters. *B*: Western blots of MEFs using antibodies to AARS and SLC1A4. The band intensity was determined using ImageJ software. The intensity of each protein was normalized to tubulin, a loading control ($n = 4$). *E*: Total amino acid concentrations in liver and WAT extracts or plasma (in nanomoles per milligram) of control and Atf4 mutant siblings ($n \geq 4$). Asx = Asp and Asn; Glx = Glu and Gln. *F*: Total and phosphorylated S6K and S6 levels, assessed with Western blots, in two sets of control and *Atf4* mutant siblings ($n = 4$).

DISCUSSION

Energy homeostasis is maintained by a dynamic interaction between several organ systems that coordinate food intake, energy stores, metabolic demands, and energy expenditure (38,39). The understanding of metabolism has fundamental and clinical importance, so efforts directed toward characterization of molecules controlling energy homeostasis and metabolism have therapeutic potential.

Here, we provide evidence that Atf4, a bZIP class transcription factor, regulates several aspects of mammalian metabolism, including fat storage, energy expenditure, and glycemic control. Some of these functional attributes may be conserved because Atf4 is expressed in the *Drosophila* fat body, a major fly metabolic organ, and flies with insertions into the *dAtf4* locus are lean and have reduced circulating carbohydrate levels.

Modernity has produced a marked increase in dietary protein intake, which in turn has epidemiological and experimental links to the current explosion of obesity and diabetes. Protein synthetic overload is often sensed in the endoplasmic reticulum, an organelle in which newly translated proteins are sorted and modified (13). The surplus in endoplasmic reticulum handling of proteins triggers the UPR, a central mechanism designed to handle endoplasmic reticulum stress (40). Accumulated evidence indicates that endoplasmic reticulum stress pathways couple obesity to metabolic dysfunctions such as diabetes (41,42).

The UPR is composed of several different limbs; each handles different aspects of the stress response (11–13). One arm of the UPR increases the availability of endoplasmic reticulum chaperons, which in turn remodel misfolded proteins into the appropriate structure. Another arm of the UPR, ISR, reduces endoplasmic reticulum workload by inhibiting bulk protein translation. A few mRNAs, such as those encoding the bZIP class transcription factors Atf4, C/EBPα, and C/EBPβ (14), respond to the ISR signal paradoxically, thereby increasing their translation. In turn, these proteins affect transcriptional programs that increase the ability of the cell to handle stress (12,42). Recent studies have illuminated a key role that these proteins and the ISR play in metabolism. For example, the ISR regulates pancreatic β-cell survival, proliferation, and insulin secretion, and the normal chow–fed insulin levels observed in the *Atf4* mutants resonate with previous descriptions (33,43).

That ISR contributes to negative outcomes produced by overindulgence may have evolutionary connections all the way to yeast (12). The TOR pathway also regulates invertebrate and vertebrate metabolism (7–10). Here, we showed that tissues derived from *Atf4* mutant mice have reduced TOR signaling, reduced expression of genes important in the intracellular concentration of amino acids, and thereby, reduced concentration of amino acids, a major TOR input. These results underscore a potential intimate relationship between Atf4 function, ISR, TOR pathway, and metabolism that could be therapeutically exploited.

ACKNOWLEDGMENTS

J.M.G. is a founder of Reata Pharmaceuticals. No other potential conflicts of interest relevant to this article were reported.

We thank Drs. Chul Ahn, Jawed Alam, Claude Desplan, Eiichi Hinoi, Xianxin Hua, Gerard Karsenty, David Ron, Bruce Spiegelman, and Charles Vinson for invaluable assistance with techniques, reagents, and manuscript preparation, as well as for helpful discussions. We thank Tammy L. Lisi for excellent technical assistance and members of the Graff lab for expert technical assistance, reagents, and insights.

REFERENCES

1. Kopelman PG. Obesity as a medical problem. Nature 2000;404:635–643
2. Krebs M, Roden M. Nutrient-induced insulin resistance in human skeletal muscle. Curr Med Chem 2004;11:901–908
3. Tremblay F, Krebs M, Dombrowski L, Brehm A, Bernroider E, Roth E, Nowotny P, Waldhausl W, Marette A, Roden M. Overactivation of S6 kinase 1 as a cause of human insulin resistance during increased amino acid availability. Diabetes 2005;54:2674–2684
4. Sarbassov DD, Ali SM, Sabatini DM. Growing roles for the mTOR pathway. Curr Opin Cell Biol 2005;17:596–603
5. Harding HP, Zhang Y, Zeng H, Novoa I, Lu PD, Calfon M, Sadri N, Yun C, Popko B, Paules R, Stojdl DF, Bell JC, Hettmann T, Leiden JM, Ron D. An integrated stress response regulates amino acid metabolism and resistance to oxidative stress. Mol Cell 2003;11:619–633
6. Um SH, D'Alessio D, Thomas G. Nutrient overload, insulin resistance, and ribosomal protein S6 kinase 1, S6K1. Cell Metab 2006;3:393–402
7. Luong N, Davies CR, Wessells RJ, Graham SM, King MT, Veech R, Bodmer R, Oldham SM. Activated FOXO-mediated insulin resistance is blocked by reduction of TOR activity. Cell Metab 2006;4:133–142
8. Teleman AA, Chen YW, Cohen SM. 4E-BP functions as a metabolic brake used under stress conditions but not during normal growth. Genes Dev 2005;19:1844–1848
9. Tsukiyama-Kohara K, Poulin F, Kohara M, DeMaria CT, Cheng A, Wu Z, Gingras AC, Katsume A, Elchebly M, Spiegelman BM, Harper ME, Tremblay ML, Sonenberg N. Adipose tissue reduction in mice lacking the translational inhibitor 4E-BP1. Nat Med 2001;7:1128–1132
10. Um SH, Frigerio F, Watanabe M, Picard F, Joaquin M, Sticker M, Fumagalli S, Allegrini PR, Kozma SC, Auwerx J, Thomas G. Absence of S6K1 protects against age- and diet-induced obesity while enhancing insulin sensitivity. Nature 2004;431:200–205
11. Wek RC, Cavener DR. Translational control and the unfolded protein response. Antioxid Redox Signal 2007;9:2357–2371
12. Ron D, Walter P. Signal integration in the endoplasmic reticulum unfolded protein response. Nat Rev Mol Cell Biol 2007;8:519–529
13. Kaufman RJ, Scheuner D, Schroder M, Shen X, Lee K, Liu CY, Arnold SM. The unfolded protein response in nutrient sensing and differentiation. Nat Rev Mol Cell Biol 2002;3:411–421
14. Oyadomari S, Harding HP, Zhang Y, Oyadomari M, Ron D. Dephosphorylation of translation initiation factor 2alpha enhances glucose tolerance and attenuates hepatosteatosis in mice. Cell Metab 2008;7:520–532
15. Rutkowski DT, Wu J, Back SH, Callaghan MU, Ferris SP, Iqbal J, Clark R, Miao H, Hassler JR, Fornek J, Katze MG, Hussain MM, Song B, Swathirajan J, Wang J, Yau GD, Kaufman RJ. UPR pathways combine to prevent hepatic steatosis caused by ER stress-mediated suppression of transcriptional master regulators. Dev Cell 2008;15:829–840
16. Lai KO, Zhao Y, Ch'ng TH, Martin KC. Importin-mediated retrograde transport of CREB2 from distal processes to the nucleus in neurons. Proc Natl Acad Sci U S A 2008;105:17175–17180
17. Yang X, Matsuda K, Bialek P, Jacquot S, Masuoka HC, Schinke T, Li L, Brancorsini S, Sassone-Corsi P, Townes TM, Hanauer A, Karsenty G. ATF4 is a substrate of RSK2 and an essential regulator of osteoblast biology; implication for Coffin-Lowry Syndrome. Cell 2004;117:387–398
18. Masuoka HC, Townes TM. Targeted disruption of the activating transcription factor 4 gene results in severe fetal anemia in mice. Blood 2002;99:736–745
19. Elefteriou F, Benson MD, Sowa H, Starbuck M, Liu X, Ron D, Parada LF, Karsenty G. ATF4 mediation of NF1 functions in osteoblast reveals a nutritional basis for congenital skeletal dysplasiae. Cell Metab 2006;4:441–451
20. Suh JM, Zeve D, McKay R, Seo J, Salo Z, Li R, Wang M, Graff JM. Adipose is a conserved dosage-sensitive antiobesity gene. Cell Metab 2007;6:195–207
21. Hoshizaki DK, Blackburn T, Price C, Ghosh M, Miles K, Ragucci M, Sweis R. Embryonic fat-cell lineage in Drosophila melanogaster. Development 1994;120:2489–2499
22. Mollereau B, Wernet MF, Beaufils P, Killian D, Pichaud F, Kuhnlein R, Desplan C. A green fluorescent protein enhancer trap screen in Drosophila photoreceptor cells. Mech Dev 2000;93:151–160
23. Ross SR, Graves RA, Greenstein A, Platt KA, Shyu HL, Mellovitz B, Spiegelman BM. A fat-specific enhancer is the primary determinant of gene expression for adipocyte P2 in vivo. Proc Natl Acad Sci U S A 1990;87:9590–9594
24. Bjorntorp P, Karlsson M, Pertoft H, Pettersson P, Sjostrom L, Smith U. Isolation and characterization of cells from rat adipose tissue developing into adipocytes. J Lipid Res 1978;19:316–324
25. Adams CM. Role of the transcription factor ATF4 in the anabolic actions of

insulin and the anti-anabolic actions of glucocorticoids. J Biol Chem 2007;282:16744–16753
26. Hewes RS, Schaefer AM, Taghert PH. The cryptocephal gene (ATF4) encodes multiple basic-leucine zipper proteins controlling molting and metamorphosis in Drosophila. Genetics 2000;155:1711–1723
27. Tanaka T, Tsujimura T, Takeda K, Sugihara A, Maekawa A, Terada N, Yoshida N, Akira S. Targeted disruption of ATF4 discloses its essential role in the formation of eye lens fibres. Genes Cells 1998;3:801–810
28. Ferrannini E, Natali A, Capaldo B, Lehtovirta M, Jacob S, Yki-Jarvinen H. Insulin resistance, hyperinsulinemia, and blood pressure: role of age and obesity: European Group for the Study of Insulin Resistance (EGIR). Hypertension 1997;30:1144–1149
29. Shimokata H, Tobin JD, Muller DC, Elahi D, Coon PJ, Andres R. Studies in the distribution of body fat: I: effects of age, sex, and obesity. J Gerontol 1989;44:M66–M73
30. Perlemuter G, Bigorgne A, Cassard-Doulcier AM, Naveau S. Nonalcoholic fatty liver disease: from pathogenesis to patient care. Nat Clin Pract Endocrinol Metab 2007;3:458–469
31. Harding HP, Zeng H, Zhang Y, Jungries R, Chung P, Plesken H, Sabatini DD, Ron D. Diabetes mellitus and exocrine pancreatic dysfunction in perk−/− mice reveals a role for translational control in secretory cell survival. Mol Cell 2001;7:1153–1163
32. Scheuner D, Song B, McEwen E, Liu C, Laybutt R, Gillespie P, Saunders T, Bonner-Weir S, Kaufman RJ. Translational control is required for the unfolded protein response and in vivo glucose homeostasis. Mol Cell 2001;7:1165–1176
33. Song B, Scheuner D, Ron D, Pennathur S, Kaufman RJ. Chop deletion reduces oxidative stress, improves beta cell function, and promotes cell survival in multiple mouse models of diabetes. J Clin Invest 2008;118:3378–3389
34. Cao H, Gerhold K, Mayers JR, Wiest MM, Watkins SM, Hotamisligil GS. Identification of a lipokine, a lipid hormone linking adipose tissue to systemic metabolism. Cell 2008;134:933–944
35. Tremblay F, Lavigne C, Jacques H, Marette A. Role of dietary proteins and amino acids in the pathogenesis of insulin resistance. Annu Rev Nutr 2007;27:293–310
36. Sancak Y, Peterson TR, Shaul YD, Lindquist RA, Thoreen CC, Bar-Peled L, Sabatini DM. The Rag GTPases bind raptor and mediate amino acid signaling to mTORC1. Science 2008;320:1496–1501
37. Hardie DG. New roles for the LKB1–>AMPK pathway. Curr Opin Cell Biol 2005;17:167–173
38. Rosen ED, Spiegelman BM. Adipocytes as regulators of energy balance and glucose homeostasis. Nature 2006;444:847–853
39. Murphy KG, Bloom SR. Gut hormones and the regulation of energy homeostasis. Nature 2006;444:854–859
40. Marciniak SJ, Ron D. Endoplasmic reticulum stress signaling in disease. Physiol Rev 2006;86:1133–1149
41. Ozcan U, Cao Q, Yilmaz E, Lee AH, Iwakoshi NN, Ozdelen E, Tuncman G, Gorgun C, Glimcher LH, Hotamisligil GS. Endoplasmic reticulum stress links obesity, insulin action, and type 2 diabetes. Science 2004;306:457–461
42. Scheuner D, Kaufman RJ. The unfolded protein response: a pathway that links insulin demand with beta-cell failure and diabetes. Endocr Rev 2008;29:317–333
43. Oyadomari S, Yun C, Fisher EA, Kreglinger N, Kreibich G, Oyadomari M, Harding HP, Goodman AG, Harant H, Garrison JL, Taunton J, Katze MG, Ron D. Cotranslocational degradation protects the stressed endoplasmic reticulum from protein overload. Cell 2006;126:727–739